JOURNAL OF SOLID STATE CHEMISTRY 119, 420–427 (1995)

Oxidation Products of $Nb_7W_{10}O_{47}$: A Transmission Electron Microscopy Study

Frank Krumeich[1]

Institut für Anorganische Chemie der Universität Bonn, Römerstrasse 164, D-53117 Bonn, Germany

Received February 8, 1995; in revised form June 19, 1995; accepted June 20, 1995

The oxidation of $Nb_7W_{10}O_{47}$ at different temperatures leads to interesting products whose structures are characterized using high-resolution transmission electron microscopy. At low oxidation temperature (T_{OX} = 500°C), fault boundaries appear which separate well-ordered microdomains exhibiting the threefold TTB superstructure of the 4:9 phase. In these boundaries, hitherto unobserved arrangements of hexagonal tunnels are ordered in a systematic way. The oxidation product obtained at 1000°C reveals a separation of WO_3 slabs which are incorporated coherently into the 4:9-type structure. After oxidation at 1200°C, the 4:9 and 2:7 phases are observed predominantly. Furthermore, the electron diffraction patterns exhibit circular diffuse scattering indicating short-range order of the filled pentagonal tunnels.

1. INTRODUCTION

The pseudobinary system Nb_2O_5/WO_3 has been of particular interest since it offers the unique possibility to study structural variations by changing gradually the oxygen/metal ratio in the range $O/\Sigma M = 2.5$ (Nb_2O_5) to 3.0 (WO_3). Three different types of structures were found (1–6): The structures of the ternary oxides in the niobium-rich as well as in the tungsten-rich region are closely related to the ReO_3 type. Changes of stoichiometry are accommodated by crystallographic shear in one (Magnéli phases, $2.9 \leq O/\Sigma M < 3.0$ with M = Nb,W (7)) or two dimensions (block structures, $2.5 \leq O/\Sigma M < 2.67$ (8)), respectively. In the medium range ($2.67 < O/\Sigma M < 2.9$), MO_6 octahedra are linked to give five-membered rings arranged around square tunnels in the same way as in the TTB structure (tetragonal tungsten bronze). Some of the pentagonal tunnels are filled with metal–oxygen strings leading to a pentagonal bipyramidal coordination of these cations. These MO_7 polyhedra share their equatorial edges with five octahedra. In the perpendicular direction, these units are joined by corner sharing forming the so-called PCs (pentagonal columns (9, 10)). The structure of Nb_2WO_8 ($O/\Sigma M = 2.67$ (11)) consists of an array of PCs.

The 4:9 phase ($4Nb_2O_5 \cdot 9WO_3$ (12)) crystallizes in a threefold superstructure of the TTB subcell caused by a systematic occupation of 4/12 of the pentagonal tunnels. This is thermodynamically a highly favored arrangement in this range of composition (13). Furthermore, three intergrowth phases between the TTB- and ReO_3-type structures exist. In the 2:7 phase (14), isolated square blocks of 4×4 octahedra are incorporated into the TTB matrix, whereas in the 4:22 and 4:50 phases, which are both non-equilibrium products (15), slabs of TTB-type are intergrown with ReO_3-type structures.

Moreover, a solid solution series $Nb_{8-n}W_{9+n}O_{47}$ ($0 < n < 5$) has been discovered recently (16). These phases crystallize also with the 4:9-type structure. They contain an amount of cations with lower valency. Through oxidation of these cations, compounds with an $O/\Sigma M$ ratio laying in between the 4:9 phase and WO_3 become accessible (17). The structural changes developed during the oxidation of $Nb_7W_{10}O_{47}$ (n = 1) at different temperatures were studied using HRTEM (high-resolution transmission electron microscopy).

2. EXPERIMENTAL

Sample Preparation

Nb_2O_5, WO_3 (both puriss., Fluka AG), and NbO_2 (prepared by reduction of Nb_2O_5 with Niob foil (18)) were mixed in the ratio 3:10:1 giving the composition $Nb_7W_{10}O_{47}$. The mixture was annealed at 1250°C for 3 days in an evacuated silica ampoule. $HgCl_2$ (about 4 mg) had been added as a mineralizer. This led to dark blue, mostly needle-shaped crystals (16). Ground material was oxidized in air at several temperatures: T_{OX} = 500°C, 5*d* (sample I), 1000°C, 3*d* (II), and 1200°C, 3*d* (III). The products were characterized by X-ray powder diffraction (Guinier method) and electron microscopy.

[1] Present address: Institut für Angewandte Chemie Berlin-Adlershof, Rudower Chaussee 5, 12484 Berlin, Germany.

0022-4596/95 $12.00

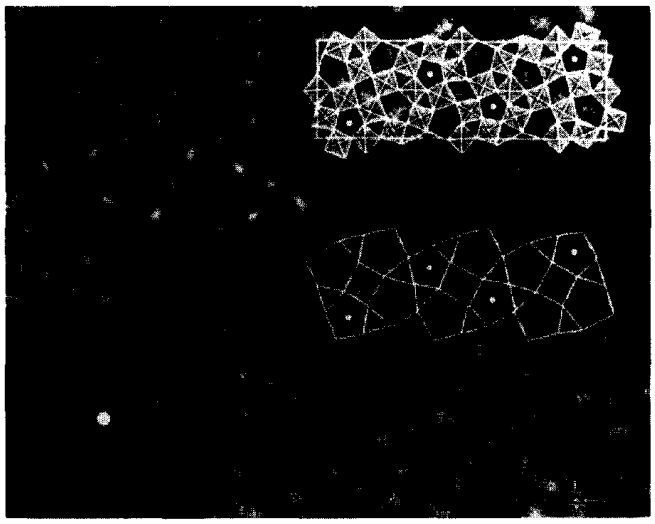

FIG. 1. (A) Electron diffraction pattern, (B) HRTEM image of $Nb_7W_{10}O_{47}$ along [001]. The structure model and the simulation (c_s = 1.2 mm, thickness d = 79 nm, defocus ε = −30 nm) are shown as insets. A simplified representation of the structure (lower right side) is used for later easier interpretation of defects: Octahedrally coordinated cations are connected by lines whereas the metal atom sites located in the pentagonal bipyramids are marked by filled circles.

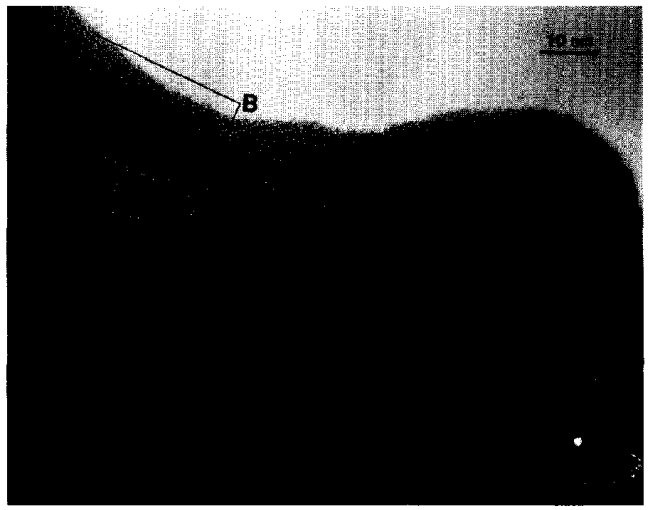

FIG. 2. HRTEM image along [001] of sample I (T_{ox} = 500°C). Planar defect (A) and displacement (B) are discussed in detail (A, Fig. 4; B, Fig. 6). The inset shows the electron diffraction pattern.

Electron Microscopy

The samples were crushed and dispersed onto holey films (carbon coated Formvar) supported on copper grids. TEM investigations were performed on a Philips CM30ST microscope operated at 300 kV (LaB_6 cathode). Thin crystal flakes were observed along [001], i.e., in *a-b* projection. The EDX analysis was done with a Philips CM200FEG microscope (200 kV, field emission gun) allowing a spatial resolved analysis of areas smaller than 1 nm^2.

3. RESULTS AND DISCUSSION

$Nb_7W_{10}O_{47}$

As reported recently (16), $Nb_7W_{10}O_{47}$ crystallizes in the orthorhombic structure of the 4:9 phase (lattice parameters: a = 1.2223, b = 3.6509, and c = 0.39376 nm). The crystal structure in projection on the *a-b* plane is observable by HRTEM (Fig. 1). Image simulations (19) have

FIG. 3. HRTEM image of sample I showing several fault boundaries which separates well-ordered domains of the 4:9-type structure. Some defects with hexagons are marked by arrows.

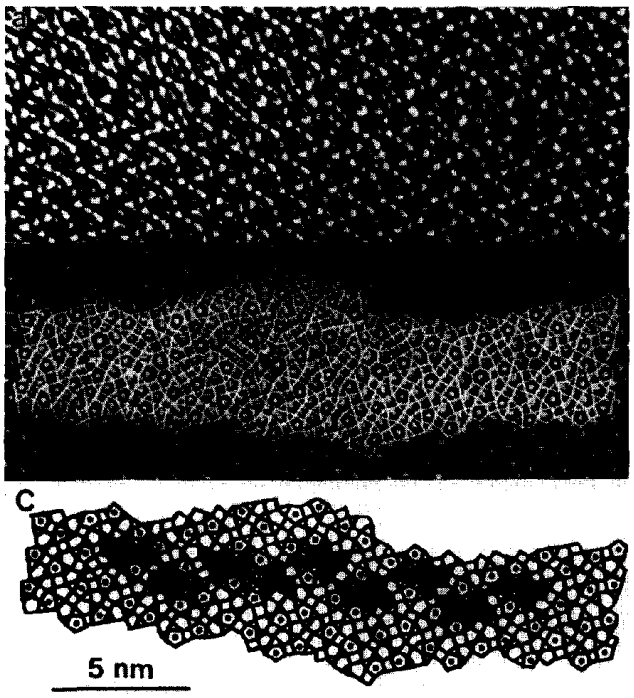

FIG. 4. (a) Enlarged area of Fig. 2 (region A) showing the presence of hexagonal tunnels, (b) structure of the fault boundary, (c) interpretation. Arrays of the ReO_3-type structure are visualized by crosses, hexagons are shaded.

been performed using the structure parameters of the 4:9 phase (12): In thin specimens (thickness <15 nm) and near the Scherzer focus, the cation sites appear as dark dots whereas bright dots correspond to the empty channels in the TTB framework (16, 20). The projection of the structure (along [001]) is fitted into the lattice image to visualize this connection (Fig. 1).

Oxidation Reactions

The initial composition of the investigated sample has been $Nb_7W_{10}O_{47}$ which can be (formally) regarded as $Nb^{4+}Nb_6^{5+}W_{10}O_{47}$. Through oxidation, a higher $O/\Sigma M$ ratio (>47:17) is reached according to

$$Nb_7W_{10}O_{47} + 1/4\ O_2 = \text{“}Nb_7W_{10}O_{47.5}\text{.”}$$

This is no longer compatible with the composition (Nb, $W)_{17}O_{47}$ required of the 4:9-type structure, even if the range of nonstoichiometry observed for the 4:9 phase (12) is taken into account. Therefore, structural changes are expected which nevertheless are not large enough to be detectable by X-ray powder diffraction; Guinier patterns of all samples oxidized at different temperatures show only the reflections of the 4:9 phase. Therefore, HRTEM was applied which appears to be the most suitable method for studying the ideal and defect structures of niobium tungsten oxides of the TTB type (5, 6, 14–16, 21, 22).

Oxidation at 500°C: The electron diffraction patterns (inset in Fig. 2) of oxidized crystals (sample I) exhibit only the reflections of the threefold TTB superstructure indicating that the 4:9-type structure is still preserved in large crystal areas. Typical lattice images along [001] (Figs. 2 and 3) give further structural information. As a characteristic feature evolved during the oxidation reaction, fault boundaries separating adjacent microdomains with well-ordered 4:9-type structure appear. These boundaries are oriented to be almost parallel to the *b*-axis of the TTB superstructure; by looking at Fig. 3 (along the *a*-axis) the continuous arrangement of the unit cells is clearly recognizable. Their linear arrangement is only interrupted by planar defects which are incorporated coherently into the matrix structure; the distribution of PCs is the same on both sides of the defect.

The fault boundaries have some special structural features in common. Rather uncommon ones are hexagonal tunnels appearing as very bright dots in the images (Figs.

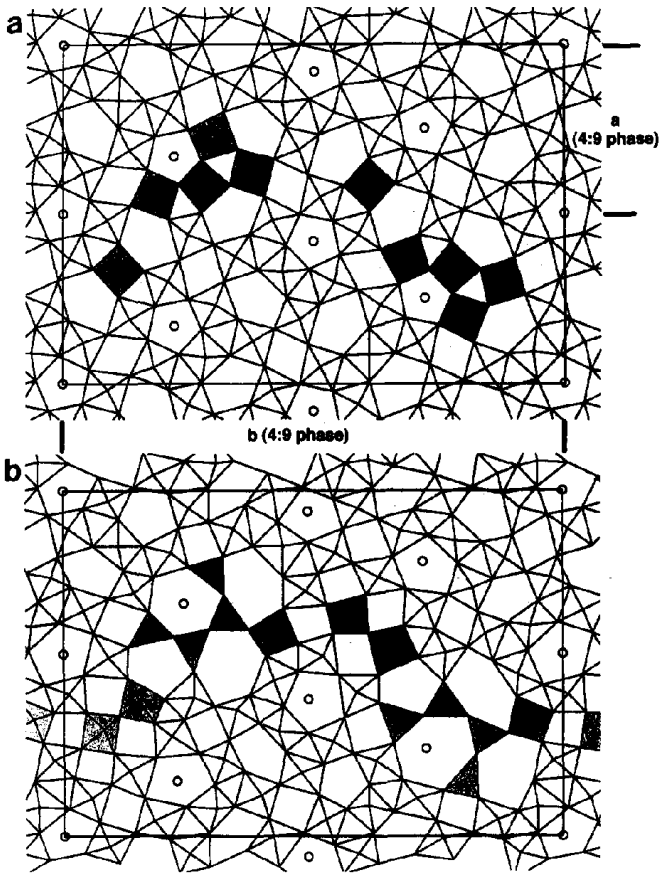

FIG. 5. Structure model of the defect before (a) and after (b) the reaction (T_{OX} = 500°C). The polyhedra affected by the structural modification are shaded.

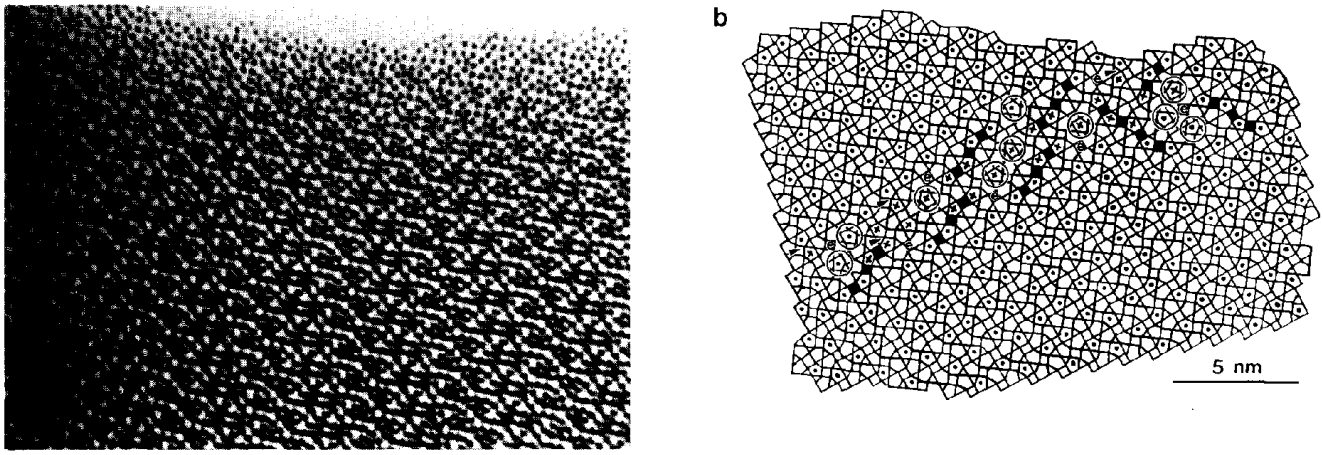

FIG. 6. (a) Enlarged area of Fig. 2 (region B) showing the perfect order of the TTB framework. (b) Interpretation which demonstrates the arrangement of pentagonal columns causing the displacement (marked by x). Filled circles indicate regular PCs. Chains of PCs are visualized by black squares between them. Isolated PCs are encircled, corner-sharing PCs marked by an arrow (in (a) and (b)), and empty TTB subcells by an e.

2 and 3). An enlarged crystal area (Fig. 4a) shows their arrangement in a defect. Two empty hexagonal tunnels recognizable as a six-membered array of dark dots are joined having two dots in common. These hexagons are connected with a third one, which is obviously occupied. They all share two cation sites with each other so that a triangle arrangement of three hexagons results. Adjacently, a square array of octahedra is recognizable.

These units are ordered in a zigzag chain along the *b*-axis. Since this particular arrangement is repeatedly observed in this and other defects, a new unit cell can be defined for its description (Fig. 5b). The cell has the same length for the *b*- and *c*-axes but is more than twice the length of the *a*-axis compared with the lattice parameters of $Nb_7W_{10}O_{47}$. This increase is caused by additional metal atoms (2 per original unit cell) built in. In spite of the longer *a*-axis, the whole defect is enclosed in the 4:9-type structure without a recognizable disturbance (Fig. 4b). Apparently, the misfit is compensated by distortions in the cation coordination in or adjacent to the defect which are not detectable in the images.

It should be noted that the TTB substructure is partly destroyed in this area by a reorganization of some five-membered rings of octahedra which form squares and hexagons in the defect (Fig. 5). If samples of similar composition are prepared by solid-state reaction of Nb_2O_5 and WO_3, only intact TTB subcells have been observed even in heavily disordered areas (14, 21). Single empty hexagonal tunnels have been observed earlier by Obayashi and Anderson in a sample of composition $Nb_2O_5:WO_3 = 2:5$ (5).

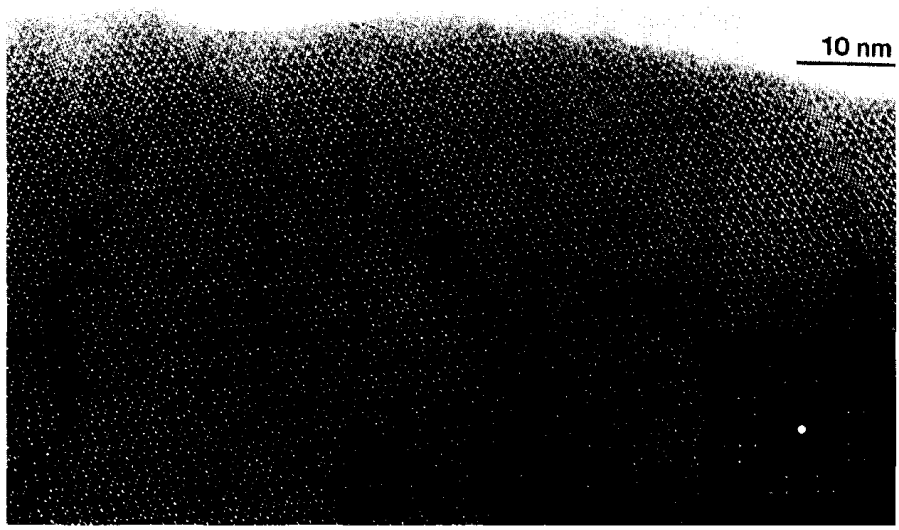

FIG. 7. HRTEM image and electron diffraction pattern of sample II (T_{OX} = 1000°C).

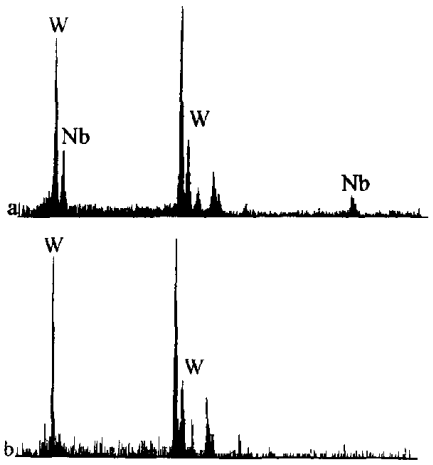

FIG. 8. EDX spectra of (a) matrix (TTB-type structure) and (b) segregation (ReO_3-type structure).

They run along [001] in a slip band. They also occur in the structures of $W_{18}O_{49}$ (23) and $W_{17}O_{47}$ (24). Moreover, the structure of hexagonal WO_3 consists of WO_6 octahedra forming only six-membered rings (25, 26). There are three hexagons connected via a triangle of octahedra whereas in the defects observed here only a single cation site is located at the joining of the three hexagons. This is not compatible with the usual octahedral coordination; trigonal bipyramids are to be assumed, a coordination rarely built either by Nb^{5+} or W^{6-} in oxides (e.g., in $LaWO_4Cl$ (27)). Since only the cation sites are detectable by HRTEM, their coordination and the $O/\Sigma M$ ratio in the defect still remain uncertain. For the same reason, the coordination of the cations located inside the filled hexagons is not unambiguously determinable. The polyhedron is not necessarily a hexagonal bipyramid since the cation site may be not exactly centered.

The filled hexagons can be formally developed out of a PC by insertion of a metal atom (Fig. 5). The origin of the additional cations is not detectable; neighbored cation sites seem to be fully occupied as one can conclude from their contrast in the HRTEM image. A possible mechanism would be the oxidation of metal ions with lower valency at the surface of the crystal and their diffusion into the crystal along the channels. A diffusion of oxygen into the crystal would be connected with a shift of cations in the crystal onto the additional sites.

Near the center of the observed area (Fig. 4), the 3×3 arrangement of octahedra is substituted by a 3×4 configuration leading to an inversion of the direction of the triangle arrangement of hexagons.

This triangle arrangement of hexagons is—in spite of being observed here for the first time—a common feature in sample I (T_{OX} = 500°C); several of them are recognizable in Figs. 2 and 3.

Even larger blocks of corner-sharing octahedra are present (Fig. 3) whereas in the TTB structure square arrangements of octahedra appear only at the joining of four pentagonal tunnels. Since more MO_6 octahedra are present, the $O/\Sigma M$ ratio of these areas is increased due to the oxidation reaction.

In contrast to the continuous arrangement of the superstructure on both sides of the fault boundaries (Figs. 2 and 3), a displacement in the 4 : 9-type structure is present in Fig. 6. The framework of the TTB substructure is not affected; it is still perfect in the whole area. The reason for the displacement is, rather, the ordering of the pentagonal columns, which is regular on both sides of the boundary but shifted. The observed displacement of 1/3 *b* is caused by changing the occupation of the pentagonal tunnels inside the boundary. In regions where the two domains are directly connected (on the right side of Fig. 6b) the displacement arises formally by a shift of metal–oxygen strings from a normally occupied pentagonal tunnel, now being empty, to an adjacent one which has been unoccupied before.

In the structure of the 4 : 9 phase, two opposite pentagonal tunnels in the TTB subcell are occupied with metal–oxygen strings so that a square arrangement of octahedra is located between two neighbored PCs (diamond linkage (9)). In this defect, different variations are present (Fig. 6b): Arrangements of three, four, and five, respectively, diamond linked PCs form short chains. Further, some PCs are isolated and connected only to empty pentagonal tunnels. Another extraordinary grouping is the connection of two neighbored PCs via a common octahedra. The displacement is probably not caused by the oxidation reaction. A displacement of 1/3 *b* had been also observed by Iijima and Allpress (14) but the structure of the boundary was more regular and includes TTB subcells with none of the pentagonal tunnels filled. Several of such empty subcells are recognizable in Fig. 6, too.

Oxidation at 1000°C: Completely different structural features arose during oxidation of $Nb_7W_{10}O_{47}$ at 1000°C (sample II). Though X-ray and electron diffraction patterns indicate only the structure of the 4 : 9 phase, the HRTEM images show a more complicated structure (Fig. 7). In analogy to sample I (T_{OX} = 500°C), the product exhibits large areas where the threefold TTB superstructure is still present. The areas between these domains consist homogeneously of square arrangements of dark dots with a distance of about 0.38 nm. The dots correspond to the cation sites of ReO_3-type structure (only corner-sharing octahedra). Because of the required stoichiometry, an accumulation of WO_3 is likely. This has been proven using energy dispersive X-ray analysis (EDX) with a small electron beam (probe size < 1.0 nm) focused on these areas. Only W is detected (Fig. 8) whereas in the domains with TTB-type structure both W and Nb are present. The oxidation at 1000°C apparently led to a phase separation according to

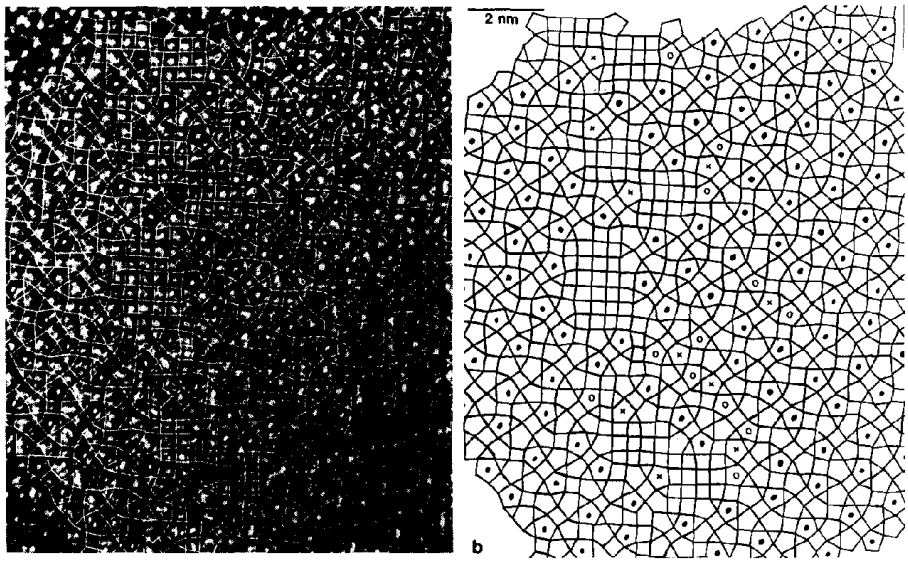

FIG. 9. (a) Enlarged area of Fig. 7. (b) Interpretation, showing the coherent intergrowth of TTB- and ReO_3-type structure. PCs of the regular structure are marked by a full circle, irregular ones by a ×, and empty PCs by empty circles.

$$8\ Nb_7W_{10}O_{47.5} = 7\ Nb_8W_9O_{47} + 17\ WO_3.$$

The regions of ReO_3-type structure are incorporated coherently in the matrix of the 4 : 9-type structure as represented by Fig. 9. The TTB subcell is a square of about 1.2 × 1.2 nm^2 which corresponds in size approximately to an arrangement of 4 × 4 corner-sharing WO_6 octahedra so that a nearly perfect match of them is given. Furthermore, the TTB structure is geometrically related to the ReO_3 type since it can be derived from a 4 × 4 block of octahedra by a 45° rotation of the four octahedra in the block center generating four pentagonal tunnels (15, 28).

While the TTB subcells at the interface always fit perfectly with the ReO_3-type slabs, the occupation of their pentagonal tunnels with metal–oxygen strings is disordered in the adjacent regions (Fig. 9). At several sites in the matrix structure, two pentagonal tunnels, which should be occupied, are empty whereas the unoccupied pentagonal tunnel, situated in between, becomes filled. This results in a decrease of the metal atom content in the neighborhood of the WO_3 segregations. Since the TTB framework is not stable with the pentagonal tunnels being all empty, some remain filled but less than in the regular 4 : 9 phase.

Two different orientation relationships between the 4 : 9-type structure and WO_3 have been observed (Fig. 7) in accordance with the two possibilities for coherent intergrowth discussed by Iijima and Allpress (21).

Oxidation at 1200°C: Electron diffraction patterns of $Nb_7W_{10}O_{47}$ crystals oxidized at 1200°C (sample III) are shown in Fig. 10. Most of the investigated crystals have kept the threefold TTB superstructure as indicated by the presence of the corresponding reflections (Fig. 10a). Additionally, nearly circular diffuse scattering occurs around the main reflections. This effect was first observed by Allpress (29) in a sample of composition $3Nb_2O_5 \cdot 8WO_3$. This observation was later explained to be caused by partial ordering of the PCs (30–32). For other crystals of sample III, a diminished state of order concerning the distribution of the PCs is observed: The superstructure reflections disappear (Fig. 10b). The HRTEM image (Fig. 11) of this crystal shows that many of the PCs are arranged to form chains via corner sharing of two octahedra (diamond linked PCs (9)). The diffuse scattering is somewhat different and not always as circular as in Fig. 10a but occasionally more structured (Fig. 10b).

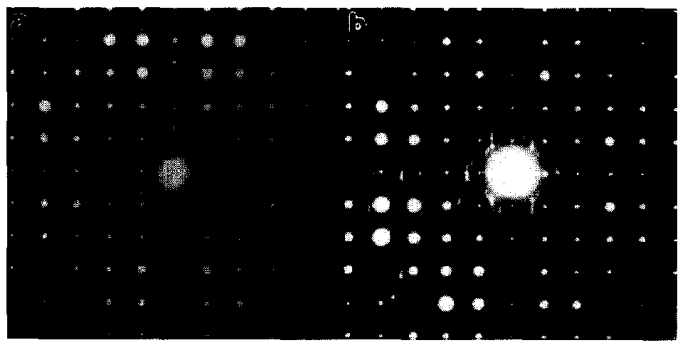

FIG. 10. Electron diffraction patterns of sample III (T_{OX} = 1200°C) exhibiting the threefold superstructure in (a), whereas in (b) only reflections of the TTB substructure are present. Additionally, circular diffuse scattering occurs in both cases.

FIG. 11. (a) HRTEM image of sample III. Unit cells of the 2:7 phase are incorporated in the matrix of the TTB-type structure. In (b), the PCs and their connection are outlined.

Typical for sample III is the appearance of isolated blocks of 4 × 4 corner-sharing octahedra spread over the whole crystal area (Fig. 11). The arrangement of empty and filled pentagonal tunnels adjacent to these blocks is exactly the same as in the structure of the 2:7 phase (14). Therefore, single columns of the 2:7 phase are incorporated into the matrix of the TTB framework. The tungsten content of the 2:7 phase is considerably higher than in the 4:9 phase so that at high oxidation temperatures (1200°C) the 2:7 phase reacts as a sink for excess tungsten oxide.

4. CONCLUSIONS

Through oxidation of $Nb_7W_{10}O_{47}$, products with an $O/\Sigma M$ ratio of 2.794 are obtained. This value is in between that of the 4:9 ($O/\Sigma M = 2.765$) and the 2:7 phase ($O/\Sigma M = 2.818$). However, the expected phase separation into these two phases occurs only at high oxidation temperature (1200°C) whereas at lower temperature (1000°C) a phase separation in WO_3 and the 4:9 phase takes place. Apparently, the 2:7 phase is thermodynamically stable only at temperatures above 1000°C. This coincides with the results of Roth and Waring (4).

At very low oxidation temperature (500°C), a metastable oxidation (33) occurs; the diffusion of cations and therefore the structural reorganization are more difficult so that nonequilibrium products result. This is indicated by the presence of structural units (e.g., triangles of hexagons) never observed in samples obtained by solid-state reactions between different amounts of Nb_2O_5 and WO_3 performed at temperatures above 1000°C. Under these conditions and starting with a mixture of the binary oxides, always perfect intergrowth between TTB and the other structure has been observed. In contrast, in the observed defects some of the TTB cells, which obviously exhibit a thermodynamically extraordinary stable arrangement, have been partly destroyed during the oxidation reaction. Similar substitution ($2\ Nb^{5+} \equiv Nb^{4+} + W^{6-}$) and oxidation experiments in the niobium-rich part of the system Nb_2O_5/WO_3 extended the region of existence of the block structures far beyond the limit at $O/\Sigma M = 2.654$ to higher W/Nb ratios (33, 34).

In both cases, oxidation at 500 as well as 1000°C, the obtained products exhibit microdomains with TTB structure which are separated by planar defects running almost in the direction of the *b*-axis. Therefore, similar first steps in the mechanism of the oxidation reactions for both temperatures are possible. In order to learn more about the mechanism, the low-temperature oxidation products obtained after different periods of reaction time should be investigated.

ACKNOWLEDGMENTS

I gratefully acknowledge Dr. M. Otten for carrying out the EDX analysis and Prof. Dr. A. Hussain for providing the source material $Nb_7W_{10}O_{47}$. I thank Prof. Dr. R. Gruehn for valuable discussions.

REFERENCES

1. R. S. Roth and A. D. Wadsley, *Acta Crystallogr.* **19,** 26, 32, 38, 42 (1965).
2. R. Gruehn, *Monatsh. Chem.* **96,** 1789 (1965).
3. S. Andersson, W. G. Mumme, and A. D. Wadsley, *Acta Crystallogr.* **21,** 802 (1966).
4. R. S. Roth and J. L. Waring, *J. Res. Natl. Bur. Stand. Sect. A* **70,** 281 (1966).
5. H. Obayashi and J. S. Anderson, *J. Solid State Chem.* **17,** 79 (1976).
6. L. Eyring and L.-T. Tai, "Treatise on Solid State Chemistry," (N. B. Hannay, Ed.), Vol. 3, p. 167. Plenum, New York, 1976.
7. P. J. England, J. Booth, R. J. D. Tilley, and T. Ekström, *J. Solid State Chem.* **44,** 60 (1982).
8. G. Heurung and R. Gruehn, *J. Less-Common Met.* **76,** 17 (1980).
9. M. Lundberg, M. Sundberg, and A. Magnèli, *J. Solid State Chem.* **44,** 32 (1982).
10. B.-O. Marinder, *Angew. Chem. Int. Ed. Engl.* **25,** 431 (1986).

11. M. Lundberg, *Acta Chem. Scand.* **26,** 2932 (1972).
12. A. W. Sleight, *Acta Chem. Scand.* **20,** 1102 (1966).
13. M. W. Viccary and R. J. D. Tilley, *J. Solid State Chem.* **104,** 131 (1993).
14. S. Iijima and J. G. Allpress, *Acta Crystallogr. Sect. A* **30,** 22 (1974).
15. S. Iijima, *Acta Crystallogr. Sect. A* **34,** 922 (1978).
16. F. Krumeich, A. Hussain, C. Bartsch, and R. Gruehn, *Z. Anorg. Allg. Chem.* **621,** 799 (1995).
17. F. Krumeich, C. Bartsch, A. Hussain, and R. Gruehn, *Vortragstag. Fachgruppe Festkörperchem.* **I,** 35 (1994)
18. A. Hussain, B. Reitz, and R. Gruehn, *Z. Anorg. Allg. Chem.* **535,** 186 (1986).
19. P. Stadelmann, *Ultramicroscopy* **21,** 131 (1987).
20. S. Horiuchi, K. Muramatsu, and Y. Matsui, *Acta Crystallogr. Sect. A* **34,** 939 (1978).
21. S. Iijima and J. G. Allpress, *Acta Crystallogr. Sect. A* **30,** 29 (1974).
22. S. Horiuchi, *Ultramicroscopy* **8,** 27 (1982).
23. A. Magnéli, *Ark. Kemi,* **1,** 223 (1949).
24. M. M. Dobson and R. J. D. Tilley, *Acta Crystallogr. Sect. B* **44,** 474 (1988).
25. B. Gerand, G. Nowogrocki, J. Guenot, and M. Figlarz, *J. Solid State Chem.* **29,** 429 (1979).
26. M. Figlarz, *Prog. Solid State Chem.* **19,** 1 (1989).
27. L. H. Brixner, H. Y. Chen, and C. M. Forris, *J. Solid State Chem.* **45,** 80 (1982).
28. B. G. Hyde and M. O'Keeffe, *Acta Crystallogr. Sect. A* **29,** 243 (1973).
29. J. G. Allpress, *Mater. Res. Bull.* **4,** 707 (1969).
30. S. Iijima and J. M. Cowley, *J. Phys. Colloq.* **38** (C7), 135 (1977).
31. R. de Ridder, G. van Tendeloo, D. van Dyck, and S. Amelinckx, *Phys. Status Solidi A* **41,** 555 (1977).
32. S. Horiuchi, K. Muramatsu, and Y. Matsui, *J. Appl. Crystallogr.* **13,** 141 (1980).
33. H. Groh, B. Meyer, and R. Gruehn, *Z. Anorg. Allg. Chem.* **497,** 56 (1983).
34. A. Hussain and R. Gruehn, *Z. Anorg. Allg. Chem.* **571,** 91 (1989).